VERA Observation of Gamma-Ray Blazar DA406

Kengo Akutagawa[1], Kenta Fujisawa[1], Kotaro Niinuma[1]

Affiliation 1: Yamaguchi University, Japan

Introduction

Nonthermal emission from relativistic jets ejected from supermassive black holes usually dominates in the wide range of electromagnetic spectrum from radio to gamma-rays.

With the recent progress of the Large Area Telescope (LAT) onboard Fermi Gamma-ray Space Telescope and new generation Cherenkov telescopes (for example, MAGIC), the number of active galactic nucleus (AGN) hosted γ-ray sources has drastically increased compared with that in the era of the Energetic Gamma-ray Experiment Telescope (EGRET)/Compton Gamma Ray Observatory (CGRO). Fig.1 and Fig.2 are gamma-ray sources was obtained by Fermi/LAT and MAGIC, respectively. Number of AGNs obtained by each system listed in table 1. However the gamma-ray emission mechanism and the location of the gamma-ray emission are under debate.[1][2]

Table 1 Number of AGN

System	Number
EGRET/CGRO	66[3]
Fermi/LAT	～900

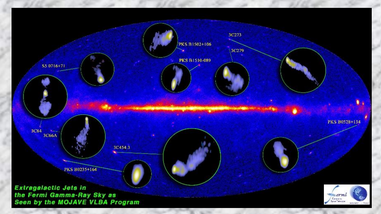

Fig.1 Fermi/LAT detected gamma-ray [4]

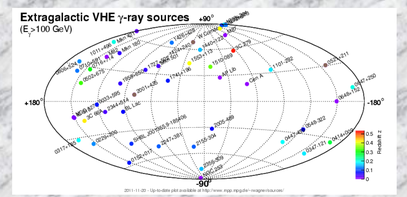

Fig.2 MAGIC Telescope detected gamma-ray[5]

Purpose

The gamma-ray emitting region is considered to be very compact because time scale of the gamma-ray variability is approximately within a day. At radio wavelengths, Very Long Baseline Interferometry (VLBI), which provides the high angular resolution possibly determines the radio counterpart of the gamma-ray emission in AGN jets.

At the moment, the high frequency VLBI monitoring is carried out in Gamma-ray Emitting Notable AGN monitoring by Japanese VLBI (GENJI) Programme for 10 AGNs.

GENJI Programme[6]

Targets : M87, BL Lac, PKS1510-089, OJ287, CTA102, NRAO0530, 3C84, 3C454.3, DA55, DA406

System : VERA-array (Mizusawa, Iriki, Ogasawara, Ishigaki-jima)

Frequency : 22 GHz

Interval : ～2 week

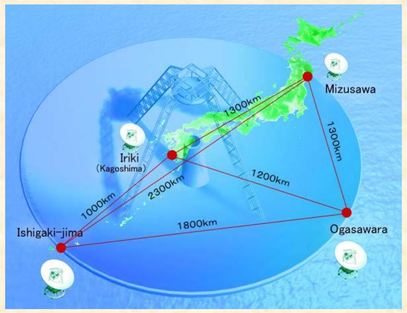

Fig.3 VERA-array (NROJ)[7]

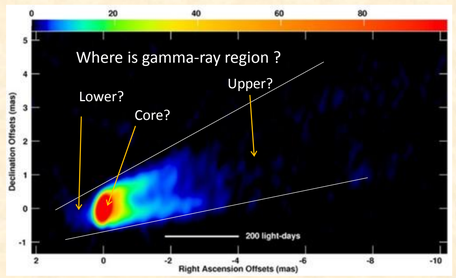

Fig.4 The Jet Base of M87 (NRAO)[8]

Target

DA406 (1611+343)

- Classified as an FSRQ (α=-0.04 : $S \propto \nu^{\alpha}$)[6][9]
- Extended jet toward south was confirmed by VLBA (1.375, 1.64, 8, 15 GHz) images.[9]
- Optical outburst was detected between 1986 October and 1987 March.[9]
- gamma-ray flux was 8 times brighter between 1992 November and 1994 November (EGRET/CGRO) than current it (Fermi /LAT)[3][6][10](see Fig.5) .

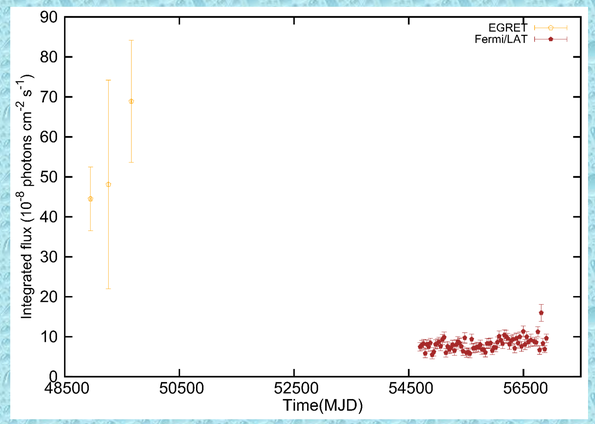

Fig.5 gamma-ray light curve of DA406

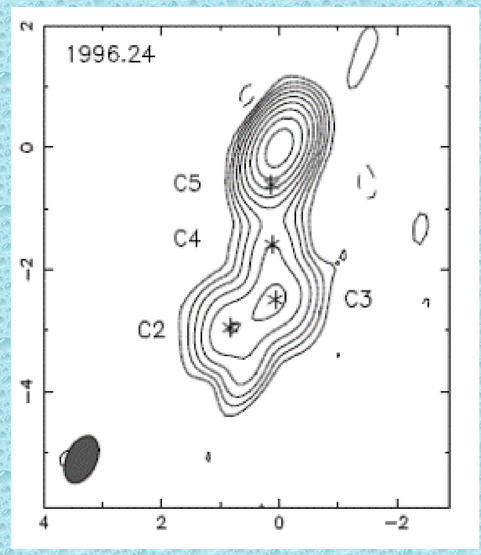

Fig.6 DA406 8GHz image[9]

Table 2 DA406 Status [6][9]

(RA , Dec)	(16h13m41s.06425, +34°12′47″.9090)
z	1.39712

Observation

DA406 is the one of GENJI targets. We use observation data of DA406. We listed typical beam size and rms noise of this data.

Table 3 beam and rms noise of DA406 data

beam size [mas ×mas]	position angle [deg]	rms noise [Jy/beam]
1.24 × 0.82	-50.7	0.00244

Result

We analyzed 21 epochs data (2010 Dec 10 – 2013 Dec 24) of GENJI using the NRAO Astronomical Image Processing System (AIPS) and Difmap software packages. Fig.7 presents one of the images made by our analysis in 2013 Mar 19. The initial contour corresponds to 3 times rms noise.

In our data analysis, we obtained 3 components (named as C0 – C2) by two-dimensional Gaussian fitting procedure in Difmap, then we measured the position of C1 and C2 with respect to the C0. We here assumed that C0 is the radio core. Distance to component C1, C2 from the core of each epoch are listed in table 4. We show motion of component C1, C2 with respect to the core in Fig.8. Apparent velocity V_{app} of each component, which is estimated by linear fitting is shown in table 5. Flux densities of each epoch are listed in table 6. We show light curve of each component in Fig.9 and compare the radio core flux with gamma-ray flux in the same period in Fig.10. We used the gamma-ray flux data listed in Fermi Science Support Center.[10]

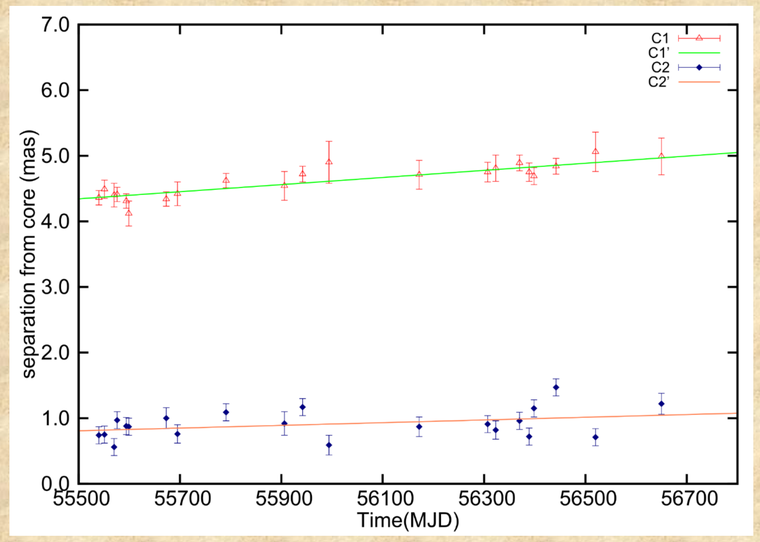

Fig.8 Motion of components of DA406

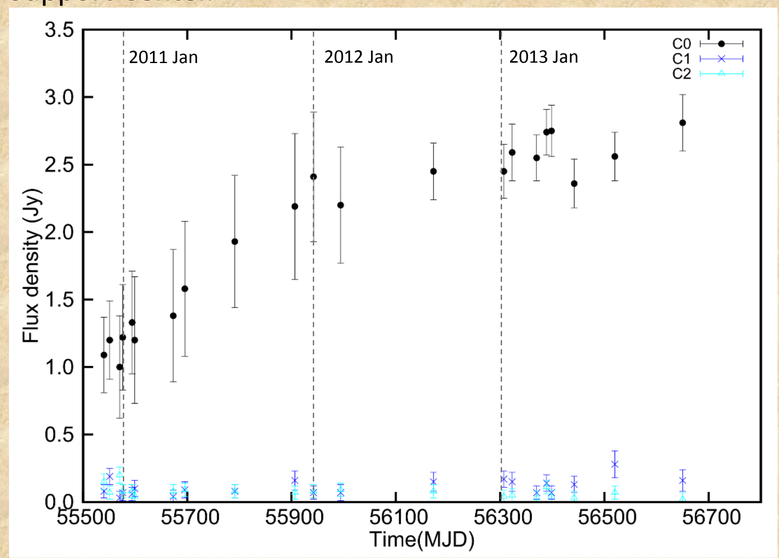

Fig.9 Light curve of DA406

Table 4 Angular separation from the radio core (C0)

		C1	C2
Date	MJD	Radius (mas)	Radius (mas)
2010/12/10	55540	4.36±0.11	0.74±0.13
2010/12/21	55551	4.49±0.14	0.75±0.13
2011/1/9	55570	4.40±0.18	0.56±0.13
2011/1/15	55576	4.41±0.11	0.97±0.13
2011/2/2	55594	4.31±0.11	0.88±0.13
2011/2/7	55599	4.12±0.19	0.87±0.13
2011/4/22	55673	4.34±0.11	1.00±0.16
2011/5/14	55695	4.42±0.18	0.76±0.14
2011/8/18	55791	4.62±0.11	1.09±0.13
2011/12/11	55906	4.54±0.22	0.92±0.18
2012/1/16	55942	4.72±0.12	1.17±0.13
2012/3/8	55994	4.90±0.32	0.59±0.15
2012/9/2	56172	4.71±0.22	0.87±0.15
2013/1/15	56307	4.75±0.15	0.91±0.13
2013/1/31	56323	4.81±0.20	0.82±0.14
2013/3/19	56370	4.89±0.12	0.96±0.13
2013/4/7	56389	4.75±0.14	0.72±0.13
2013/4/16+17	56398.5	4.69±0.13	1.15±0.13
2013/5/30	56442	4.84±0.12	1.47±0.13
2013/8/16	56520	5.06±0.30	0.71±0.13
2013/12/24	56650	4.99±0.28	1.22±0.16

Table 6 Flux density of each component

		C0	C1	C2
Date	MJD	Flux density (Jy)	Flux density (Jy)	Flux density (Jy)
2010/12/10	55540	1.09±0.28	0.08±0.05	0.15±0.06
2010/12/21	55551	1.20±0.29	0.19±0.06	0.07±0.05
2011/1/9	55570	1.00±0.38	0.03±0.05	0.20±0.06
2011/1/15	55576	1.22±0.39	0.07±0.06	0.08±0.05
2011/2/2	55594	1.33±0.38	0.06±0.05	0.08±0.05
2011/2/7	55599	1.20±0.47	0.10±0.06	0.04±0.05
2011/4/22	55673	1.38±0.49	0.04±0.05	0.08±0.05
2011/5/14	55695	1.58±0.50	0.09±0.06	0.09±0.05
2011/8/18	55791	1.93±0.49	0.08±0.05	0.08±0.05
2011/12/11	55906	2.19±0.54	0.16±0.07	0.07±0.05
2012/1/16	55942	2.41±0.48	0.07±0.05	0.08±0.05
2012/3/8	55994	2.20±0.43	0.07±0.06	0.09±0.05
2012/9/2	56172	2.45±0.21	0.15±0.07	0.08±0.05
2013/1/15	56307	2.45±0.20	0.17±0.06	0.04±0.05
2013/1/31	56323	2.59±0.21	0.15±0.07	0.05±0.05
2013/3/19	56370	2.55±0.17	0.07±0.05	0.03±0.05
2013/4/7	56389	2.74±0.17	0.14±0.06	0.11±0.05
2013/4/16+17	56398.5	2.75±0.19	0.07±0.05	0.04±0.05
2013/5/30	56442	2.36±0.18	0.13±0.06	0.03±0.05
2013/8/16	56520	2.56±0.18	0.28±0.10	0.07±0.05
2013/12/24	56650	2.81±0.21	0.16±0.08	0.02±0.05

Table 5 Apparent velocity of each component (c =3.0*10^8 m/s)

	C1	C2
V_{app} (m/s)	5.56±0.64 c	2.11±1.27 c

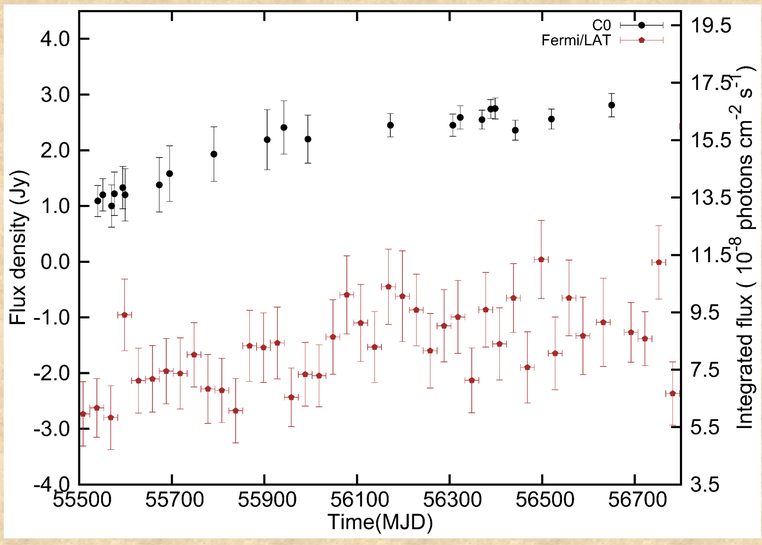

Fig.10 Light curve of C0 and Fermi/LAT

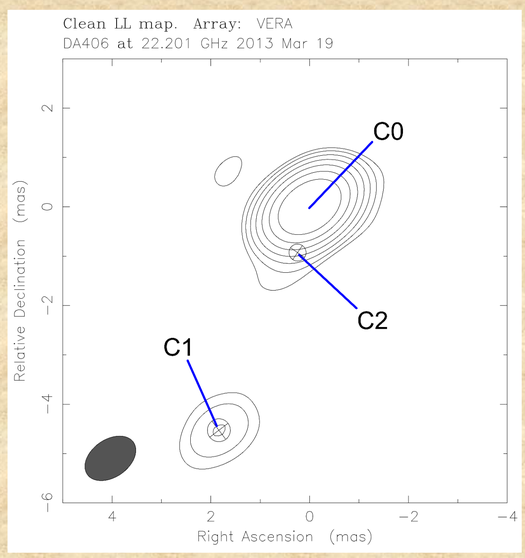

Fig.7 DA406 image (Map peak 2.55 Jy/beam, beam size 1.14 ×0.763 mas, Contours 0.0139 Jy/beam ×(1 2 4 8 16 32 64))

Discussion

At first, Fig.8 and table 5 show farther component C1 moves faster than closer one C2. If we assume apparent velocities of these components in the case of they come out from radio core are the same. Component may accelerate so as to be separated from the core.

In Fig.9, the radio core represent increase of the flux density within a year.

In Fig.10, we found that intensity of 22GHz and γ-ray is increasing with a similar trend.

Based on these observational facts, we conclude that γ-ray emitting region of DA406 is in radio core and the origin of radio emission and gamma-ray emission is the same.

Reference

[1] Marscher. et al.,2010ApJ...710L.126M
[2] Orienti, M. et al.,2013MNRAS.428.2418O
[3] Hartman, R. C. et al., 1999ApJS..123...79H
[4] http://www.nasa.gov/mission_pages/GLAST/news /radio_telescope.html
[5] https://www.mpp.mpg.de/~rwagner/sources/
[6] Nagai H. et al., 2013PASJ...65...24N
[7] http://veraserver.mtk.nao.ac.jp/system/index-e.html
[8] http://images.nrao.edu/589
[9] Piner, B.G.et al., 1997ApJ...479..684P
[10] http://fermi.gsfc.nasa.gov/ssc/